Smart 3D-FISH: Automation of Distance Analysis in Nuclei of Interphase Cells by Image Processing

Michael Gué,[2] **Cédric Messaoudi,**[1] **Jian Sheng Sun,**[2] **and Thomas Boudier**[1]*

[1] UMR 168 CNRS-Institut Curie, Paris, France
[2] USM 0503, UMR 5153 CNRS-MNHN, U 565 INSERM, Département "Régulations, Développement et Diversité Moléculaire,"
Muséum National d'Histoire Naturelle, Paris, France

Background: Detection of fluorescent probes by fluorescence in situ hybridization in cells with preserved three-dimensional nuclear structures (3D-FISH) is useful for studying the organization of chromatin and localization of genes in interphase nuclei. Fast and reliable measurements of the relative positioning of fluorescent spots specific to subchromosomal regions and genes would improve understanding of cell structure and function.
Methods: 3D-FISH protocol, confocal microscopy, and digital image analysis were used.
Results: New software (Smart 3D-FISH) has been developed to automate the process of spot segmentation and distance measurements in images from 3D-FISH experiments. It can handle any number of fluorescent spots and incorporate images of $4'$,6-diamino-2-phenylindole counterstained nuclei to measure the relative positioning of spot loci in the nucleus and inter-spot distance. Results from a pilot experiment using Smart 3D-FISH on *ENL*, *MLL*, and *AF4* genes in two lymphoblastic cell lines were satisfactory and consistent with data published in the literature.
Conclusion: Smart 3D-FISH should greatly facilitate image processing and analysis of 3D-FISH images by providing a useful tool to overcome the laborious task of image segmentation based on user-defined parameters and decrease subjectivity in data analysis. It is available as a set of plugins for ImageJ software. © 2005 Wiley-Liss, Inc.

Key terms: fluorescence; confocal microscopy; three-dimensional fluorescence in situ hybridization; image processing; segmentation; ImageJ

Cell imaging techniques are integral to successful life science studies and, at the dawn of the post-genome sequencing era, techniques that permit the accurate localization of genes and their products within cells and tissues will be in ever-increasing demand. The rapidly developing field of cell imaging techniques has greatly contributed to the current understanding of cell structure and function. Fluorescence in situ hybridization (FISH) is used to study the organization and positioning of chromosomes, subchromosomal regions, and/or specific sequences such as genes or RNA in cellular preparations by hybridization of probes with complementary sequences in cells. It is important that after fixation of cells on glass slides, they retain, as near as possible, their in vivo morphology (1–3). A protocol of cell fixation based on paraformaldehyde has been developed to perform FISH in the three-dimensionally (3D) preserved structure of nuclei in cells in which the relative position of chromatin and genes are quite well conserved (4). This technique, named 3D-FISH, has opened the way to study the organization of the chromatin in interphase nuclei.

Individual chromosomes have been shown to occupy discrete regions in interphase nuclei, called chromosome territories (CTs) (5,6). The global position of chromosomes in interphase nuclei seems to be conserved through cell division (7) and even along evolution (8,9). This localization depends on the size of the chromosomes (10) and the density of genes carried by the chromosomes (11). Further, observations have shown that the spatial organization of the genome is specific to cell lineage (12).

Recently, several investigations have provided evidence that CTs are not randomly distributed but are partially oriented in cell nuclei (13). However, the precise organization of CTs, in particular the positioning of genes inside CTs, is not fully understood. This organization may depend on functional processes such as transcription, replication, repair, and recombination processes.

Relative positions of genes inside nuclei and their dynamics in interphase cells could play a major role in chromosomal rearrangements, i.e., reciprocal translocation or inversion. For instance, some studies about chromatin organization in interphase nuclei have indicated

that the spatial proximity of genes could be a key factor in the induction of translocations (14–18). Further, the differences in relative position of CTs in different cell lineages could contribute to the large variety of translocations, especially in hematologic cancer (19).

To further address this relation, the spatial distribution of CTs, or intergenic distances between genes potentially involved in chromosomal translocations, must be accurately analyzed. The 3D-FISH technique allows one to produce 3D images where real gene-to-gene distances can be measured with better precision than with classic 2D-FISH images (20). In a 2D-FISH experiment, such a task is quite straightforward, but it often, if not always, leads to erroneous data due to the localization of spots (genes) on different focal planes (2D projection). In a 3D-FISH experiment, the analysis is a heavy workload and complex task for the biologist. Obtaining reliable data involves multiple steps: visual inspection for selecting a region of interest, manual segmentation, and detection of the center of spots corresponding to the localization of genes. Because hundreds of image stacks need to be analyzed for reaching statistical significance, the analysis is very time consuming. Further, and importantly, it has the bias of the user's subjectivity and is not well reproducible or reliable.

The goal of the present work is to provide an user-friendly software to improve the quality of rather high throughput analysis of 3D-FISH images and the subsequent positioning of genes and measurement of intergenic distances. With the help of this software, named Smart 3D-FISH, image stacks corresponding to hundreds of cells can be automatically analyzed overnight on a desktop computer. The software can be used on any FISH studies, including 2D studies. It can analyze images with a virtually unlimited number of color channels (probes). The results are saved as text files that can be directly incorporated into standard spreadsheet software. In the first part, the procedure of image processing and software are described. The second part deals with the validation of these procedures and software in a 3D-FISH experiment involving three genes (three color probes) and 4′,6-diamino-2-phenylindole (DAPI) counterstained nuclei.

This new software has been successfully applied in a 3D-FISH experiment aimed at measuring the 3D radius distribution of genes involved in acute leukemia, namely *MLL*, *AF4*, and *ENL*, in two lymphoblastic cell lines. Smart 3D-FISH is available as a set of plug-ins for the image analysis ImageJ software (21). It can be freely downloaded from http://www.snv.jussieu.fr/~wboudier/softs.html.

MATERIALS AND METHODS
Cell Culture and Karyotype

Two human cell lines were chosen due to their near diploid karyotype. A human B-cell precursor leukemia (NALM-6) was kindly provided by Lagneaux L. (Brussels, Belgium) with the karyotype 46(43-47)<2n>XY, t(5;12)(q33.2;p13.2); and we purchased a human B lymphoblastoid cell line (IM-9, DSMZ Braunschweig, Germany) that has an apparently normal karyotype 46(44-46)<2n>XX. These two lymphoblastic cell lines were cultured in RPMI-1640 medium supplemented with 10% fetal calf serum, 1% L-glutamine, in the absence of antibiotics, at 37°C in a humidified atmosphere containing 5% CO_2.

DNA Probes

Bacterial artificial chromosome/phage artificial chromosome (BAC/PAC) clones were obtained from the Resources for Molecular Cytogenetics (RMC) database (http://www.biologia.uniba.it/rmc/) in Italy: CTD-217A21 for the *MLL* gene (22) and RP11-476C8 for the *AF4* gene. RP11-2344B19 for the *ENL* gene was purchased from Invitrogen (Carlsbad, CA, USA). Clones were grown in LB medium with appropriate antibiotics: kanamycin (50 μg/ml) for PAC clones or chloramphenicol (12.5 μg/ml) for BAC clones. DNA extraction was carried out according to the protocols in the RMC database. The probes of *MLL*, *AF4*, and *ENL* genes were labeled by nick translation by incorporating fluorophore-tagged nucleotides dUTP-Alexa 488 (Molecular Probes Europe, Netherlands), dUTP-Cy5, and dUTP-Cy3 (Amersham, Buckinghamshire, UK), respectively. Four hundred nanograms of labeled probes, 10 μg of human cot-1-DNA, and 5 μg of salmon sperm DNA were mixed in medium containing 50% deionized formamide, 2× standard saline citrate (SSC), 10% dextran sulfate, and 0.5 M of sodium phosphate dibasic:sodium phosphate monobasic (5:1).

3D-FISH Experiment

A dense cell suspension in 1× phosphate buffer saline (PBS) was applied to slides coated with poly-L-lysine for 10 min to allow cell adhesion. Cells were then fixed in buffered 4% paraformaldehyde in 1× PBS for 10 min to preserve the native 3D structure of the nuclei and then washed 3 times for 5 min in 1× PBS. During all procedures, air drying was carefully avoided. Cells were permeabilized with 0.5% Triton X-100 and 0.5% saponin in 1× PBS for 15 min. After a bath in 20% glycerol in 1× PBS for 20 min at room temperature, cells were freeze-thawed by briefly dipping the slides three times in liquid nitrogen. Cells were treated with 400 μg/ml of RNase A (Roche Diagnostics, Myelan, France) for 15 min at 37°C. After a 5-min bath in 0.1 N HCl, cells were washed in 2× SSC for 5 min and incubated in 50% formaldehyde and 2× SSC, pH 7.5, for 1 h. The probe preparation was then dropped onto slides. Cells and probes were simultaneous denatured at 75°C for 8 min. Cells were incubated overnight at 37°C in a humidified chamber. Post-hybridization washes were performed a first time in 50% formaldehyde and 2× SSC, pH 7.2, at 42°C, 3 times for 15 min and a second time in 0.1× SSC, pH 7.2, at 60°C, 3 times for 15 min. Nuclei were counterstained with DAPI at 0.2 μg/ml. Slides were mounted in Vectashield medium.

Image Acquisition and Measurement

Confocal microscopy was carried out using a TCS confocal imaging system (Leica Instruments, Heidelberg, Germany) equipped with a 63× objective. For Alexa 488, Cy3, and Cy5 excitations, an argon-krypton ion laser and

a helium-neon ion laser were adjusted to 488, 568, and 647 nm, respectively. A biphotonic device was used for DAPI excitation. For each optical section, four fluorescence images were acquired in a sequential mode (i.e., Cy5, Cy3, Alexa 488, and DAPI). The confocal pinhole was adjusted to allow a minimum field depth. The focus step between sections was generally 0.35 μm (which corresponds to the optimal optical resolution) and the *XY* pixelization was set to 100 nm. Focal series were then processed to produce a single composite image file (stack). Typically, a stack of 40 confocal planes was acquired.

Total DNA is counterstained by DAPI dye. Due to the biphotonic acquisition mode on the microscope, images from the DAPI channel are shifted. To register them with other images from other color channels, DAPI images were translated. The *XY* translation was then implemented to automatically shift the area of interest for the DAPI channel.

The radius of each nucleus was estimated according to a spherical approximation by measuring the volume of the nucleus, counterstained by DAPI, in 3D-FISH images. The distance of genes to the nuclear center was then measured and expressed as a percentage of the nuclear radius. Statistical analyses were performed using Student's *t* test with an α value of 0.05.

Image Processing

All algorithms were implemented in JAVA and can be run as plugins on the free multiplatform ImageJ software. A possible procedure for 3D processing is to apply 2D processing in a slice-by-slice manner. However, slice-by-slice processing tends to remove weak signals that could be considered pixels of noise in the 2D slice but that are part of a signal in 3D images. Hence, all implemented procedures were adapted to work with voxels (i.e., incorporating *X*, *Y*, and *Z* directions) in 3D images. The implemented algorithms can work with real 3D color images. A 3D color image is considered as a set of unlimited numbers of 3D gray-level images (each corresponding to a different color channel). For a set of images less than or equal to three channels, the standard red/green/blue (RGB) color code is used for display. For more than three colors, each 3D gray-level image is distributed into at least one red, green, or blue channel; a 3D RGB image is then calculated by summing the contribution of all the 3D single gray-level images.

Noise Filtering and Spot Segmentation

Figure 1 shows the flow chart of the overall algorithm. The first step in processing the images is to remove background noise. The median filter is well suited for salt-and-pepper noise; for a general reference on image processing, see Russ (23) and Castleman (24). This filter, adapted to 3D images, is used with a neighborhood of radius equal to 2 pixels. Then a 3D Top Hat filter is applied to enhance the spots against the background and decrease the level of background noise. This filter is defined by: Top Hat(Im) = Im − Max7(Min7(Im)), as previously described (25). The second step is the segmentation of the spots. The central pixels inside each spot are determined to correspond to pixels whose value is greater than 99.95% of the histo-

gram, i.e., with a value greater than v (v is defined as 99.95% of all pixel values in the range $[0 - v]$). This value of 99.95% of the histogram was computed by estimating the volume of one spot and considering that a stack could comprise up to four spots.

More precisely, the pixel whose intensity is maximal in the 3D stack, but greater than 99.95% of the histogram, is detected. This pixel is a seed from where a spot will be segmented. A local threshold is computed corresponding to mean + sigma of the pixels belonging to three lines in the three directions (*X, Y, Z*) passing through the detected center of the spot. The seed is extended, by 3D connectivity, to adjacent pixels whose value is greater than this local threshold to form an object. If the final segmented object is touching one border of the image in the *X-Y* plane, then it is removed. These procedures (detection of maximum pixel and 3D connectivity) are applied until no more unsegmented pixels have a value greater than 99.95% of the histogram. The segmentation is performed on all the different stacks except for the DAPI channel.

For the DAPI channel, a special segmentation is automatically performed. The radius of the first median filter applied to reduce the noise is increased to a radius of 4 pixels to obtain a more homogeneous signal. The stack is then thresholded using the "Isodata" algorithm (26).

For spots and DAPI segmentation, a 3D mathematical morphologic closing procedure is applied followed by a 3D mathematical morphologic opening procedure (radius 2 for gene images, radius 4 for nucleus DAPI images) to remove very small objects, fill holes, and make shape look more compact.

Analysis and Validation of Segmentation

A first analysis of the validity of the segmentation is done after the application of the median filter (Fig. 1). If the computed signal-to-noise ratio (SNR; maximum − minimum value of gray level in the image stack) is lower than a threshold fixed by the user, further measurements will be discarded into an invalidated spots file. A second analysis of the validity of the segmentation is based on the volume and number of objects. The list of segmented objects is analyzed to detect whether or not the segmented objects correspond to gene spots. Segmented objects with volumes smaller than the minimal volume ($minV_1$), fixed by the user, are removed. In the same way, objects with volumes larger than the maximum volume ($maxV_1$) are removed. They are often due to an incorrect experimental procedure or acquisition mode. Then, if the number of spots exceeds the value fixed by the user (two in the present work), the segmentation is considered invalid and further measurements will be performed, but the results will be redirected into the invalidated spots file.

In all cases, results of measurements are saved as text files. Two text files are created; the first text file will store the results for correct segmentation, and the other one will store the results for incorrect segmentation, i.e., where one parameter (SNR, volume and number of spots) does not correspond to the values fixed by the user. In this last case, annotations will indicate the nature of the problem.
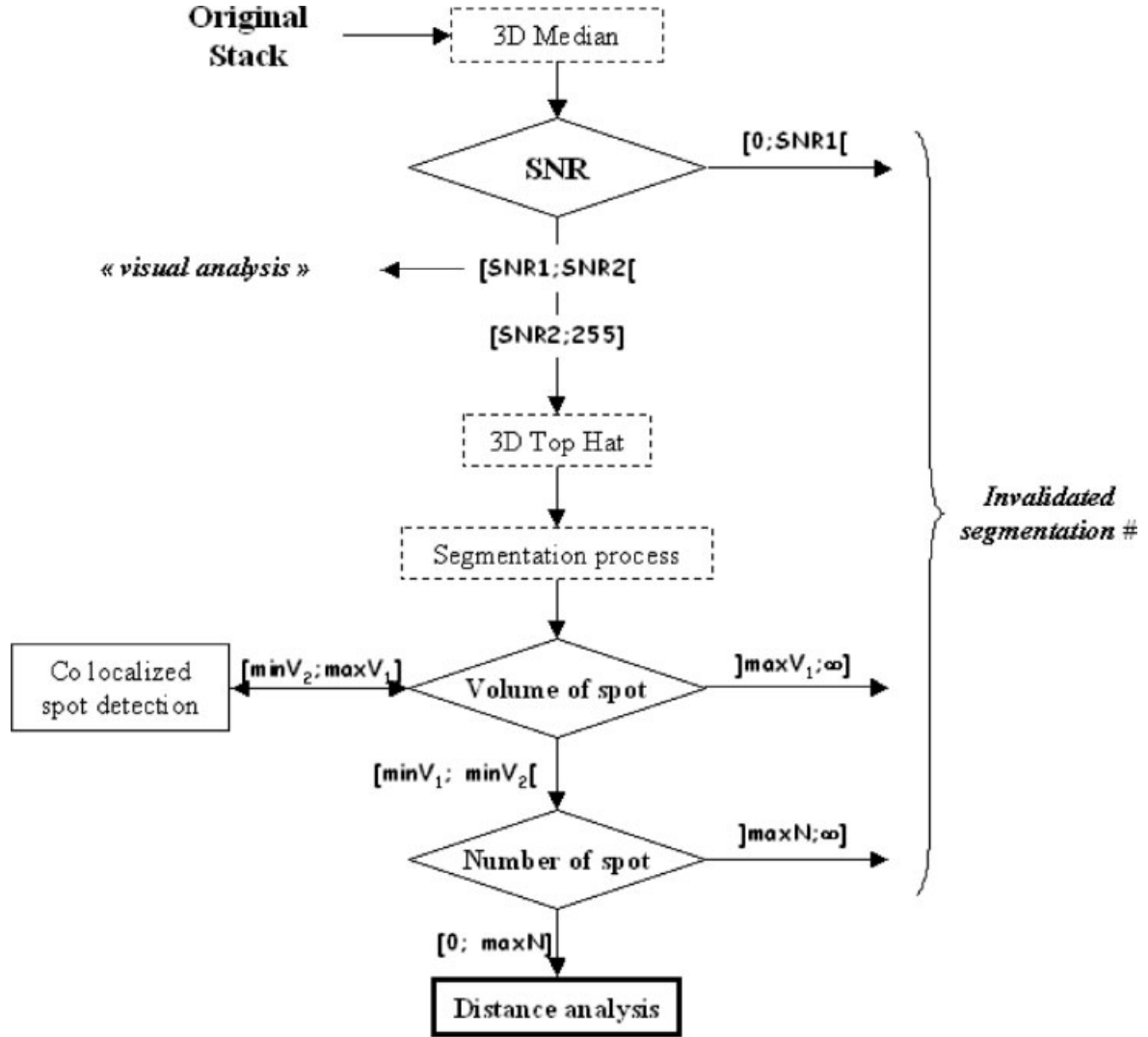
Fig. 1. Flow chart of Smart 3D-FISH software. Threshold values corresponding to signal-to-noise ratio ($SNR1$, $SNR2$), spot volume ($minV_1$, $minV_2$, $maxV_1$), and number of spots are set by the user and can be saved in a configuration file. A 3D median filter is applied to original images before SNR calculation. If SNR is between 0 and SNR1 [0;SNR1[, the results will be directed into the invalidated spots file (#). If the SNR is between SNR1 and SNR2 [SNR1;SNR2], the results will be labeled as "visual analysis" for further in-depth analysis. A 3D Top Hat filter is then performed on the filtered stack. The segmentation process is validated by checking the volume and number of objects. If the volume of an object is smaller than the minimum spot size ($minV_1$), the object will be discarded (not shown on flow chart). If the volume is between the minimum size of two colocalized spots ($minV_2$) and the maximum volume of one spot ($maxV_1$), the process of separation will be run. If this process cannot find two colocalized spots, the original object is labeled as a "large spot" in the final results. If the volume of an object is larger than the maximum volume ($maxV_1$), this object is discarded from the analysis but will be displayed on the final segmented image for visual control, and the results will be directed into the invalidated spots file. The number of objects is then checked to finalize the segmentation analysis process. The invalidated spots file contains all results where the image SNR is lower than the $SNR1$ value or the volume of one spot is larger than $maxV_1$ or the number of spots is larger than the limit value fixed by the user ($maxN$). All segmented image stacks are saved for further visual examination.

Spot Separation Procedure

Figure 2 illustrates the spot separation procedure. The mathematical morphologic procedures may not be sufficient to separate two closely located spots. Close spots may be merged into one big spot with a volume roughly twice the average volume of one spot. The user can fix the minimum volume that may correspond to a merged spot ($minV_2$). The slices of the stack containing the object are projected along the Z axis onto a 2D plane to find local maxima that may correspond to the center of the two merged spots. The obtained projection is then smoothed

so that local maxima are more easily detected. If two or more local maxima are encountered, they are separated into two clusters using a k-means algorithm. If the center of the two clusters are farther apart more than a fixed distance, corresponding approximately to the diameter of one spot ($dist$), the object can be separated into two smaller objects. The centers of these two clusters are the new x and y coordinates. The z value of the two new objects is determined as the center of the primary segmented object along the Z axis for the x and y coordinates of each new spot. Pixels of the primary big object are then resegmen-
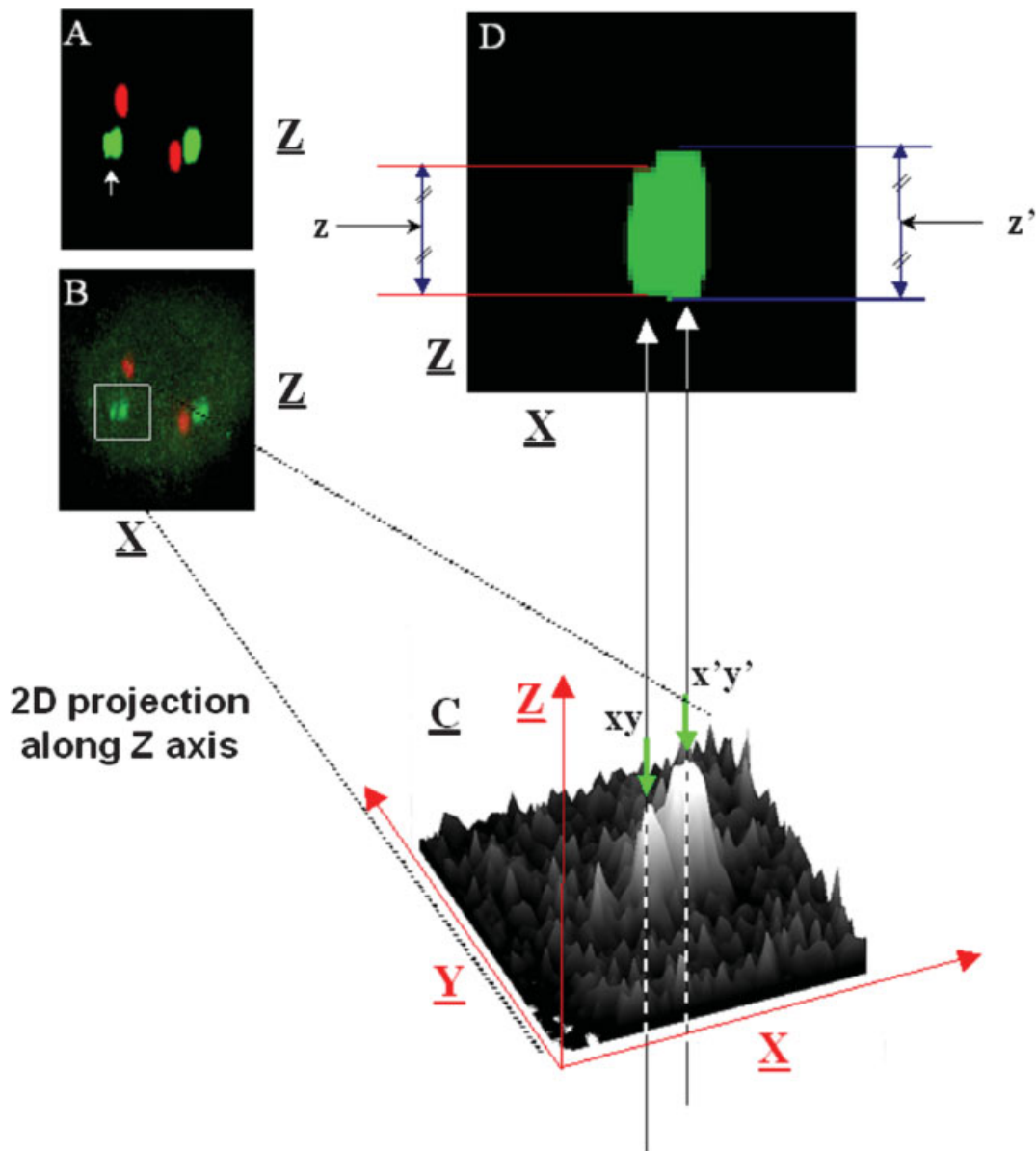
Fig. 2. Spot separation process. **A:** 2D projection along the *Y* axis of the segmented image stack. White arrow indicates one object whose volume is between $minV_2$ and $maxV_1$ (Fig. 1) before the spot separation process. **B:** The same 2D projection proves that the object detected as one object is, in reality, composed of two colocalized spots. **C:** To distinguish these two spots on the segmented image, a 2D projection is performed along the *Z* axis to enhance the signal corresponding to each spot. Then local maxima are detected to find *XY* coordinates of each spot. If two local maxima are detected farther apart than the *dist* (see text), the two spots are separated. **D:** On the segmented stack, *Z* coordinates of each new spot are then detected along the *Z* axis (from *XY* coordinates previously detected) as the middle of the segmented object.

ted according to their distance to the center of these two new objects. If the primary object cannot be split into two objects, it is kept in the list of segmented objects but will be annotated as "large spot."

RESULTS
Image Processing and Software Description

From the confocal microscope, a stack is obtained where cells are present for all channels (corresponding to probe colors). An integrated utility was developed to help

biologists select an area of interest delimiting one cell and save all the various channels in different directories. Stacks corresponding to *ENL*, *AF4*, and *MLL* genes were saved on the red, yellow, and green channels, respectively. An additional blue channel for DAPI counterstaining of nuclei was also used to determine the relative positioning of different probes to the center of nucleus.

The segmentation procedure was inspired by detection of microcalcification in mammograms using a RH-maxima procedure (27), with the exception that all the procedures were performed in 3D and not in a slice-by-slice

manner. One important issue is the threshold setting to find a seed for a spot. A high threshold corresponding to the 99.95% of the histogram was chosen. An automatic determination of this value was tested based on histogram analysis (supposing the presence of two or three classes correspond to the spots, the hybridization procedure noise, and the background) but was found to depend strongly on the image acquisition; we then chose to keep the fixed value of 99.95% as the threshold. However, to control the quality of the segmentation procedure, a set of parameters entered by the user is used to control the validity of the segmented objects (Fig. 1).

The software is comprised of several utilities that can be used separately or run consecutively thanks to a configuration file. A configuration file is created to process many directories, each containing as many subdirectories as number of colors. A certain number of parameters must be entered by the user such as the resolution in *X-Y* and *Z*. For each color, two SNR values are to be entered, namely *SNR1* and *SNR2*. The SNR reflects the difference between the maximum and minimum of stack intensity, computed after 3D median filtering procedure, and indicates the presence of spots. However, a high SNR does not necessary reflect the presence of bright spots, as would be the case if the offset of the microscope was not optimal. Nevertheless, a low SNR implies a small range of values and, in most cases, the absence of spots or spots insufficiently bright to be detected. If the computed SNR is below *SNR1*, the results will be directed into an invalidated spots file. If the image SNR is between *SNR1* and *SNR2*, the stack is labeled as "visual analysis" for further in-depth analysis. Then for each channel, parameters are to be filled such as the maximum volume for one spot (*maxV_1*), the minimum volume for one spot (*minV_1*), and the minimum volume that corresponds to the possible colocalization of two spots (*minV_2*). These parameters are used to check the quality of segmented objects. When the microscope setting is not optimal, the software may detect a large object raised from background pixels. In this case, the segmented object will be too large and will not be considered a spot. The next parameter, the number of spots, checks the validity of the segmentation by directing the results into an invalidated spots file when the number of spots is too large. The value of this parameter can be changed by the user according to the context of investigation (e.g., cell lines with nondiploid karyotype). The last parameter corresponds to the minimum distance between two colocalized spots (*dist*).

Parameters implemented in the software (SNRs, volume of each spot, number of spots, and distance between two spots close to each other) can be adjusted for each channel to take into account variations of fluorescence characteristics of each probe and their hybridization quality, post-hybridization washes, microscope parameter settings, and karyotype of cell lines. In the present work, adequate setting of these parameters was obtained by averaging values tested to give satisfactory results on more than 100 stacks: SNR values of 80 and 120, minimum spot volume of 2.5 μm^3, minimum spot volume for two "colo-

calized" spots of 5 μm^3, distance of 7 pixels between colocalized spots, and maximum spot number of 2.

Separation of two closely located spots (Fig. 2) was the most complicated process. Nevertheless, we were able to correctly split merged spots in most cases (70% to 80%), except when the spots were one on top of the other along the *Z* axis (<2% of cases).

The results of the distance measurements are saved in two different files. One file corresponds to segmentations that were labeled as correct and saved in a validated spots file, and the other corresponds to segmentations that were labeled as incorrect and saved in an invalidated spots file. The results are available as a text file where all the information of the spots is indicated, such as the center position of the spot, its area, and its volume. The distances between homologous and nonhomologous genes, between genes and center of nuclei, and angle between homologous genes with center of nuclei were also computed.

Validation and Statistical Significance

A pilot 3D-FISH study was performed to validate the above described procedures and software by determining with statistical significance the positioning of *ENL*, *AF4*, and *MLL* genes to the center of nuclei and their intergenic distances in two lymphoblastic cell lines. Only their positioning (distance) to the center of nucleus is reported here. Intergenic distances will be reported in a future publication.

A 3D-FISH experiment was performed in NALM-6 and IM-9 leukemia lymphoblastic cell lines. These two human B-cell lines were chosen because they have near diploid, normal karyotype. Figure 3 shows an example of consecutive central slices out of a 40-image stack with different color channels corresponding to *ENL* (red), *AF4* (yellow), and *MLL* (green) genes in NALM-6 cells. Perfect correlation was obtained for FISH spots (corresponding to labeled genes) and DAPI counterstaining in blue (corresponding to nucleus) on the original stacks compared with the segmented stacks. Statistical analysis, performed on more than 150 cells that corresponded to a total number larger than 450 image stacks, showed good sensibility (probability to have a correctly segmented image in the validated spots file) and good specificity (probability to have an incorrectly segmented image in the invalidated spots file) with values of 98% (427 of 435) and 99% (101 of 102), respectively. Note that the five of eight stacks that were not correctly segmented on validated spots file displayed two spots one on top of the other along the *Z* axis.

For all distances (gene to center of nucleus and gene to gene), comparison between 3D and 2D distances, which were computed on a 2D projection, was performed (Table 1), and more than 93% of measurements changed. In 44% of cases, measurements were underestimated by at least 10% and, in some cases, the ratio changed by more than 90%. The same comparison was performed on the angle between homologous genes and the center of the nucleus. More than 50% of angles were changed by a value greater than 10 degrees. Average distances for each cell lines were computed for 3D and 2D distances (Table 2). Results
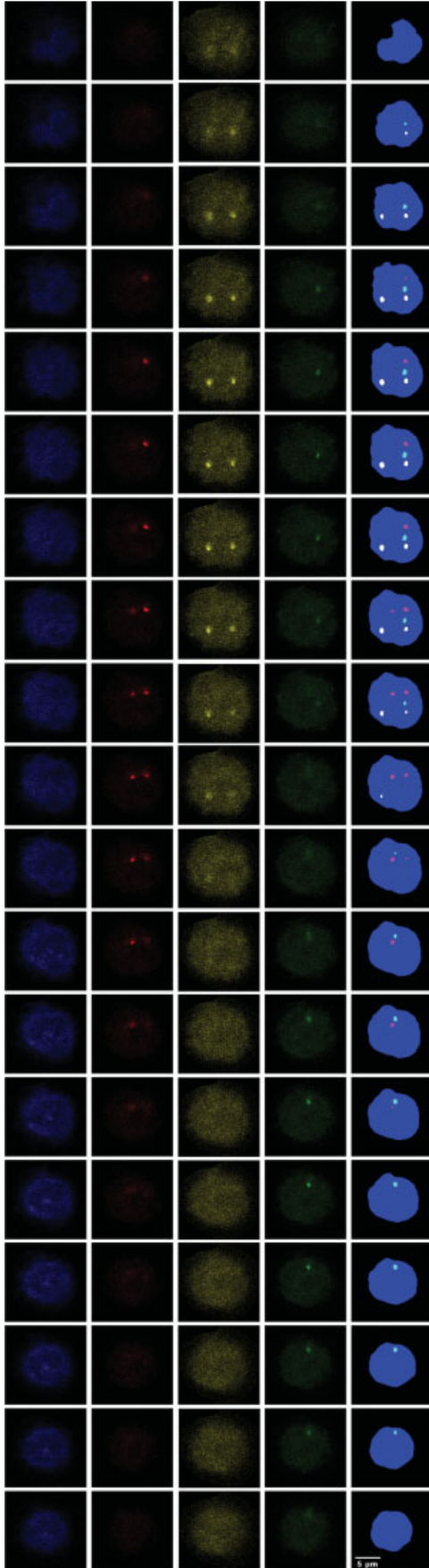
FIG. 3. Example of four-color image stack from a 3D-FISH experiment. Distance between slices was 0.35 μm. The leftmost column shows images corresponding to DAPI counterstaining of nucleus. The second, third, and fourth columns show images corresponding to hybridization signals of two the loci of the *ENL* gene (19p13.3), *AF4* gene (4q21), and *MLL* gene (11q23), respectively. The rightmost column, named "segmented and merged," displays the combination of all segmented images.

Table 1
*Ratio Between 2D and 3D Measurements for G-G and G-C Distances**

	2D/3D ratio			
	1–0.9 (1)	0.9–0.5	0.5–0.1	0.1–0
G-C (n = 2,034)	54.5 (5.8)	37.8	7.6	0.1
G-G (n = 4,068)	55.5 (6.45)	36.6	7.6	0.1

*G-C, gene-to-nuclear center distances; G-G, gene-to-gene distances. Percentage of measurements, for which ratio is equal to 1, is presented in parentheses.

showed significative differences between 3D and 2D gene-to-center measurements in both cell lines. Distribution of 3D distances between loci of each gene (*MLL*, *AF4*, and *ENL*) with the center of nucleus in NALM-6 and IM-9 cell lines was analyzed. Results are shown in Figure 4 and Table 2. Radius distribution of the *AF4* and *ENL* genes was significantly similar in the two cell lines ($P < 0.0001$). However, a small difference in radius distribution was noted for the *MLL* gene. It was noted that the distribution along the nucleus radius showed that the *ENL* gene has a more central nucleus localization than the *MLL* and *AF4* genes. The *AF4* gene appears to be more peripheral.

DISCUSSION

Visual comparison between segmented image stacks and original images stacks showed no difference in position, size, and number of spots. These observations validated the segmentation procedure. The procedure of spot separation implemented in this software is quite complex but seems to give quite a satisfactory outcome. However, it strongly depends on the minimal distance between two spots (*dist*). The separation of two spots along the *Z* axis could be implemented by projecting candidate spots onto *xy* and *yz* planes. However, due to the relative small number of colocalized spots in this position and the optical distortion along the *Z* direction, this procedure was not implemented. The interest of this separation could be to study the position of all genes through the cell cycle, taking into account newly replicated spots. The comparison between 3D and 2D measurements showed an underestimation of distances in 2D condition, which could lead to erroneous interpretation. Further, thanks to real 3D measurements, exceptional events have a better probability to be detected than on 2D projections.

Our 3D-FISH experiments show that the *ENL* gene localized on chromosome 19 occupies the most central nuclear localization, whereas the *AF4* gene (on chromosome 4) appears to be more peripheral, probably near the nuclear membrane. The *MLL* gene (on chromosome 11)

Table 2
2D Versus 3D Radial Distances* for the AF4, MLL, and ENL Genes in Two Cell Lines

	3D		2D		P	
	IM-9	NALM-6	IM-9	NALM-6	IM-9	NALM-6
AF4	83.2 ± 1.5	81.7 ± 1.3	74.4 ± 1.9	68.9 ± 1.8	0.00041	<0.0001
MLL	74.7 ± 1.6	71.9 ± 1.7	67.6 ± 1.9	60.3 ± 2.1	0.004	<0.0001
ENL	61.2 ± 1.6	62.9 ± 1.6	55.8 ± 1.7	55.0 ± 1.8	0.025	0.001

*Values are expressed as average distances (percentage of nuclear radius) $\pm$ standard error. Student's t test was applied with $\alpha = 0.05$.

has an intermediate localization. These observations reflect dynamics of loci inside CTs. They are consistent with previous studies showing that chromosomes 19 in interphase nuclei are more central (28). The relative positioning of chromosomes in nuclei is organized according to their size (10): the smaller chromosomes (e.g., chromosomes 19) are more centrally localized than the larger ones (e.g., chromosome 4). No significant difference in radial distribution was observed for the *AF4* and *ENL* genes between these two lymphoblastics cell lines. As expected, these results corroborated a relative conserva-
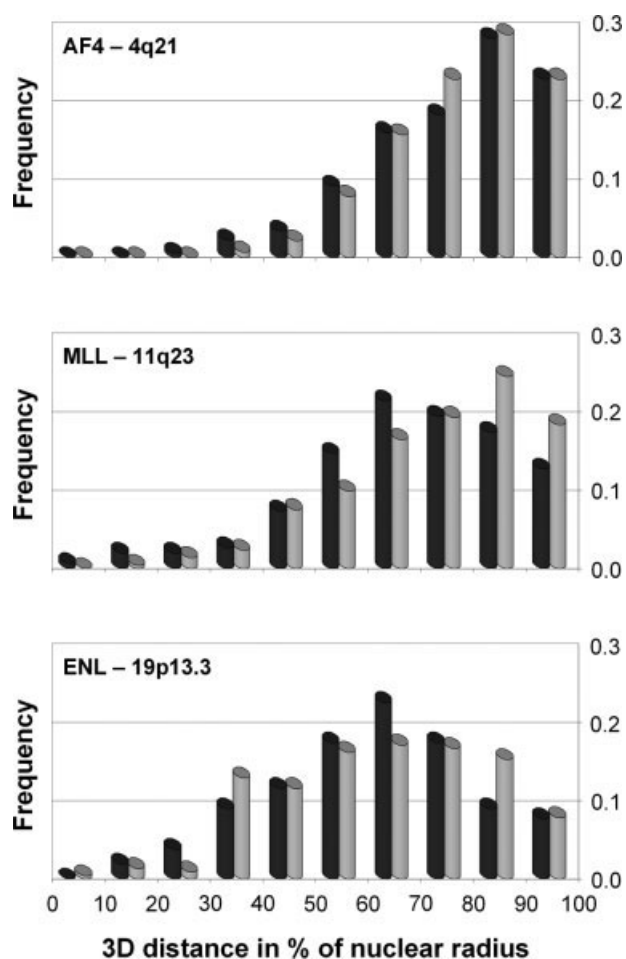

Fig. 4. Radial distribution of gene-to-nuclear center distances for the *AF4*, *MLL*, and *ENL* genes (from top to bottom) in NALM-6 (black bars) and IM-9 (gray bars) lymphoblastic cell lines. Distances are expressed as a percentage of the nuclear radius.

tion of CT organization for a given cell line (12). However, the radial distribution of the *MLL* gene seems to be slightly different on these two lymphoblastic cell lines. The *MLL* gene seems to be more centrally located in the NALM-6 than in the IM-9 cell line. NALM-6 is a human B-cell precursor in contrast to the IM-9 cell line. Cell differentiation may cause a subtle difference in nuclear organization of the *MLL* gene, as has been shown for other genes in the literature (29,30).

In conclusion, it seems that the image processing procedures and parameter settings implemented in the software allow satisfactory image data processing and analysis. Other 3D-FISH experiments carried out in different cell lines with additional probes are also satisfactory (data not shown). Smart 3D-FISH is new software that has been developed to automate the process of spot segmentation and perform distance measurements in 3D-FISH. It can handle virtually any number of spots and color channels for intergenic distance measurements. It can also incorporate the images from DAPI channel (total DNA of nucleus) to measure distances of genes to a nuclear center. A 3D-FISH experiment carried out on *ENL*, *MLL*, and *AF4* genes in two lymphoblastic cell lines has shown self-consistent data and corroborated previously reported data in the literature concerning the organization of chromosomes inside nuclei. Visual comparison of original image stacks with segmented image stacks by Smart 3D-FISH provided satisfactory detection of all spots, with a sensitivity of 98%. The software is user friendly and robust in use. Smart 3D-FISH is available as a set of plug-ins for ImageJ software at http://www.snv.jussieu.fr/~wboudier/softs. html.

It should greatly facilitate image processing and analysis by providing a useful tool to overcome the laborious task of 3D image measurements based on user-defined parameters and decrease subjectivity in data analysis.

LITERATURE CITED

1. Manuelidis L. Individual interphase chromosome domains revealed by in situ hybridization. Hum Genet 1985;71:288–293.
2. Zirbel RM, et al. Evidence for a nuclear compartment of transcription and splicing located at chromosome domain boundaries. Chromosome Res 1993;1:93–106.
3. Lichter P, et al. Delineation of individual human chromosomes in metaphase and interphase cells by in situ suppression hybridization using recombinant DNA libraries. Hum Genet 1988;80:224–234.
4. Solovei I, et al. Spatial preservation of nuclear chromatin architecture during three-dimensional fluorescence in situ hybridization (3D-FISH). Exp Cell Res 2002;276:10–23.
5. Manuelidis L. A view of interphase chromosomes. Science 1990;250:1533–1540.
6. Zorn C, et al. Laser UV microirradiation of interphase nuclei and post-treatment with caffeine. A new approach to establish the arrangement of interphase chromosomes. Hum Genet 1976;35:83–89.
7. Gerlich D, et al. Global chromosome positions are transmitted through mitosis in mammalian cells. Cell 2003;112:751–764.
8. Tanabe H, et al. Non-random radial arrangements of interphase chromosome territories: evolutionary considerations and functional implications. Mutat Res 2002;504:37–45.
9. Tanabe H, et al. Evolutionary conservation of chromosome territory arrangements in cell nuclei from higher primates. Proc Natl Acad Sci USA 2002;99:4424–4429.
10. Sun HB, et al. Size-dependent positioning of human chromosomes in interphase nuclei. Biophys J 2000;79:184–190.
11. Cremer T, et al. Chromosome territories, interchromatin domain compartment, and nuclear matrix: an integrated view of the functional nuclear architecture. Crit Rev Eukaryot Gene Exp 2000;10:179–212.
12. Parada LA, et al. Tissue-specific spatial organization of genomes. Genome Biol 2004;5:R44.
13. Amrichova J, et al. Nuclear and territorial topography of chromosome telomeres in human lymphocytes. Exp Cell Res 2003;289:11–26.
14. Lukasova E, et al. Localisation and distance between ABL and BCR genes in interphase nuclei of bone marrow cells of control donors and patients with chronic myeloid leukaemia. Hum Genet 1997;100:525–535.
15. Kozubek S, et al. The topological organization of chromosomes 9 and 22 in cell nuclei has a determinative role in the induction of t(9,22) translocations and in the pathogenesis of t(9,22) leukemias. Chromosoma 1999;108:426–435.
16. Neves H, et al. The nuclear topography of ABL, BCR, PML, and RARalpha genes: evidence for gene proximity in specific phases of the cell cycle and stages of hematopoietic differentiation. Blood 1999;93:1197–1207.
17. Nikiforova MN, et al. Proximity of chromosomal loci that participate in radiation-induced rearrangements in human cells. Science 2000;290:138–141.
18. Roix JJ, et al. Spatial proximity of translocation-prone gene loci in human lymphomas. Nat Genet 2003;34:287–291.
19. Alcobia I, et al. The spatial organization of centromeric heterochromatin during normal human lymphopoiesis: evidence for ontogenically determined spatial patterns. Exp Cell Res 2003;290:358–369.
20. Kozubek S, et al. Influence of cell fixation on chromatin topography. Anal Biochem 2000;282:29–38.
21. Rasband W. National Institute of Health, Bethesda, MD, USA. ImageJ, http://rsb.info.nih.gov/ij.
22. von Bergh A, et al. A DNA probe combination for improved detection of MLL/11q23 breakpoints by double-color interphase-FISH in acute leukemias. Genes Chromosomes Cancer 2000;28:14–22.
23. Russ J. The image processing handbook. 4th ed. Boca Raton: CRC Press; 2002.
24. Castleman K. Digital image processing. Saddle Brook, NJ: Prentice-Hall; 1996.
25. Netten H, et al. FISH and chips: automation of fluorescence dot counting in interphase cell nuclei. Cytometry 1997;28:1–10.
26. Ridler T, Calvard S. Picture thresholding using an iterative selection method. Syst Man Cybernetics 1978;630–632.
27. Shmidt M, Préteux F. Un nouvel algorithme en morphologie mathématique: les rh-maxima et rh-minima. 2D Image Symp 1986;2:469–475.
28. Croft JA, et al. Differences in the localization and morphology of chromosomes in the human nucleus. J Cell Biol 1999;145:1119–1131.
29. Weiler KS, Wakimoto BT. Chromosome rearrangements induce both variegated and reduced, uniform expression of heterochromatic genes in a development-specific manner. Genetics 1998;149:1451–1464.
30. Vermaak D, Wolffe AP. Chromatin and chromosomal controls in development. Dev Genet 1998;22:1–6.